Some refinements to the most recent simple time-dependent theory of tropical cyclone intensification and sensitivity

Yuqing Wang*

International Pacific Research Center and Department of Atmospheric Sciences, School of Ocean and Earth Science and Technology, University of Hawaii at Manoa, Honolulu, Hawaii

Zhe-Min Tan, and Yuanlong Li

School of Atmospheric Sciences, Nanjing University, Nanjing, China.

June 12, 2022 (submitted)
August 23, 2022 (revised)
September 27, 2022 (final)
Dateline

Submitted to ***Journal of the Atmospheric Sciences***

*Corresponding author: Prof. Yuqing Wang
Room 404A, IPRC/SOEST
University of Hawaii at Manoa
1680 East-West Road
Honolulu, HI 96822
Email: yuqing@hawaii.edu

Abstract

Several key issues in the simple time-dependent theories of tropical cyclone (TC) intensification developed in recent years remain, including the lacks of a closure for the pressure dependence of saturation enthalpy at sea surface temperature (SST) under the eyewall and the definition of environmental conditions, such as the boundary-layer enthalpy in TC environment and the TC outflow-layer temperature. In this study, some refinements to the most recent time-dependent theory of TC intensification have been accomplished to resolve those issues. The first is the construction of a functional relationship between the surface pressure under the eyewall and the TC intensity, which is derived using the cyclostrophic wind balance and calibrated using full-physics axisymmetric model simulations. The second is the definition of TC environment that explicitly includes the air-sea temperature difference. The third is the TC outflow-layer temperature parameterized as a linear function of SST based on global reanalysis data. With these refinements, the updated time-dependent theory becomes self-contained and can give both the intensity-dependent TC intensification rate (IR) and the maximum potential intensity (MPI) under given environmental thermodynamic conditions. It is shown that the pressure dependence of saturation enthalpy at SST can lead to an increase in the TC MPI and IR by about half of that induced by dissipative heating due to surface friction. Results also show that both MPI and IR increase with increasing SST, surface enthalpy exchange coefficient, environmental air-sea temperature difference, and decreasing environmental boundary-layer relative humidity, but the maximum IR is insensitive to surface drag coefficient.

Significance statement: A new advancement in the recent decade is the development of simple time-dependent theories of tropical cyclone (TC) intensification, which can provide quantitative understanding of TC intensity change. However, several key issues in these simple time-dependent theories remain, including the lacks of a closure for the pressure dependence of saturation enthalpy at sea surface temperature under the eyewall and the definition of environmental conditions. These are resolved in this study with several refinements, which make the most recent time-dependent theory of TC intensification self-contained and practical.

1. Introduction

The development of simple time-dependent theories of tropical cyclone (TC) intensification is fundamental to the quantitative understanding of TC intensity change. Emanuel (2012) is the first among others who have attempted to develop such a theory based on the boundary layer momentum and entropy budget equations and the assumptions of an axisymmetric vortex in thermal wind balance and neutral slantwise moist convection in the eyewall ascent in the free atmosphere above the boundary layer. Ozawa and Shimokawa (2015) also constructed a time-dependent theory of TC intensification by assuming a TC as a Carnot heat engine with the hypothesis that the TC intensifies when the energy production rate associated with the sea surface enthalpy flux is greater than the surface frictional dissipation rate. We can simply consider the former as a dynamically based theory and the latter as an energetically based theory. Although both theories seem to capture the main processes of TC intensification, they mathematically show the maximum intensification rate at the incipient stage of a TC, which contrasts with observations as indicated by Xu and Wang (2015, 2018a), who found a maximum intensification rate at intermediate TC intensities (with the maximum sustained 10-m wind speed around 35–40 m s^{-1}) for TCs over the North Atlantic and the western North Pacific.

To allow the realistic intensity dependence of intensification rate in the theoretical model as in observations, Wang et al. (2021a) introduced a dynamical efficiency into the energetically based theory of TC intensification, which is parameterized as the normalized inner-core inertial stability of the TC. With the parameterized dynamical efficiency, the modified energetically based time-dependent theory can reproduce the observed and numerically simulated intensity dependence of TC intensification rate as found in observations by Xu and Wang (2015 and 2018a). This modified energetically based theory also can quantitatively capture the intensity dependence of the possible or potential intensification rate of real TCs as recently evaluated by Xu and Wang (2022). In a later study, Wang et al. (2021b) derived a new simple time-dependent equation of TC intensification, which is dynamically based as that developed by Emanuel (2012). In his theory, Emanuel (2012) assumed that the moist isentropic surface and the absolute angular momentum surface are congruent in the eyewall ascent, which is assumed to be moist neutral to convection. However, Peng et al. (2018) found that this assumption is satisfied in the later intensification stage but not in the early intensification stage when the TC is weak. In Wang et al. (2021b), the moist neutral condition in the eyewall ascent is relaxed by introducing an *ad-hoc* parameter to measure the extent to which the moist neutral condition of the eyewall ascent can be approximated.

Wang et al. (2021b) showed that although the *ad-hoc* parameter and the dynamical efficiency introduced in Wang et al. (2021a) were explained by different physical reasons, they share the same mathematical form and play a key role in limiting the TC intensification rate during the incipient and early intensification stages when the TC is weak. This suggests that the energetically based and the dynamically based approaches result in a unified time-dependent theory of TC intensification. In a more recent study, Wang et al. (2022) further considered the dissipative heating due to surface friction as an internal heating source in the slab boundary-layer entropy budget equation, with the latter being assumed to be in thermodynamic quasi-equilibrium, namely a quasi-balance between the radial advection of entropy and the surface entropy flux under the eyewall. They showed that with dissipative heating, the theory can better reproduce the observed shift of maximum intensification rate towards relatively higher TC intensity.

The latest version of the simple time-dependent equation of TC intensification including the effect of dissipative heating has the following form, namely Eq. (8) in Wang et al. (2022):

$$\frac{\partial V_m}{\partial \tau} = \frac{\alpha C_D}{h}\left\{AV_{MPI}^2 - \left[1 - \gamma A \varepsilon\left(1 - \frac{\delta C_k}{2C_D}\right)\right] V_m^2\right\}, \tag{1}$$

$$V_{MPI}^2 = \frac{C_k}{C_D}\varepsilon(k_0^* - k_b)|_{r_m}, \tag{2}$$

where V_m is the maximum near-surface wind speed of the TC (namely the current TC intensity), τ is time, α is the reduction factor of the near-surface wind speed from the depth mean boundary layer wind speed at the radius of maximum wind (RMW, r_m), h ($\approx$ 2000 m) is the depth of the slab boundary layer, $\varepsilon = \frac{T_s - T_o}{T_s}$ is the thermodynamic efficiency without considering the dissipative heating (Emanuel 1986), T_s and T_o are the sea surface temperature (SST) and outflow-layer air temperature, C_k and C_D are the surface exchange coefficient and the surface drag coefficient, respectively, k_0^* and k_b are the sea surface saturation enthalpy at T_s and the enthalpy of the boundary layer air at the RMW, respectively, γ $(1 \geq \gamma \geq 0)$ is a parameter to control the percentage of dissipative heating due to surface friction that is used to warm the atmospheric surface layer and the remaining part (1-γ) is transferred to the ocean surface waves and ocean mixing layer, as advocated by Kieu (2015), δ is a parameter (0 or 1) to track the possible effect of dissipative heating on surface heat flux when dissipative heating is considered $(1 \geq \gamma > 0)$ as recently advocated by Edwards (2019), and lastly, the *ad-hoc* parameter A satisfies $0 \leq A \leq 1$, which measures the extent to which the moist neutral condition of the eyewall ascent is satisfied (Wang et al. 2021b).

In Eq. (2) the maximum potential intensity (MPI) without the inclusion of dissipative heating is time-dependent because the sea surface saturation enthalpy at the RMW depends on the local surface air pressure, which is a function of TC intensity. In addition, In Eq. (1), the *ad-hoc* parameter is also a function of the time-dependent MPI and TC intensity (Wang et al. 2022, see discussion in section 2 below). Although the replacement of the time-dependent MPI in Eq. (2) by the steady-state MPI does not yield large errors (Wang et al. 2022), it is better to develop a closure to allow a full consideration of the time-dependence of TC intensification theory, making it self-consistent. Furthermore, the MPI in Eq. (2) is also a function of the environmental thermodynamic conditions, which is given from independent calculations in our previous applications (Xu and Wang 2022; Wang et al. 2022). Actually, the MPI is largely determined by the environmental parameters, such as the boundary-layer relative humidity and air-sea difference in the TC environment (Bister and Emanuel 2002; Xu et al. 2019a,b). As a closed theory, it is better to explicitly include the environmental parameters as inputs, making the theory self-contained.

The main objective of the present study is to make the simple time-dependent theory of TC intensification recently documented in Wang et al. (2022) self-consistent and self-contained with some refinements. In addition to the introduction of some refinements, we will also address the following two issues: given favorable environmental conditions, whether a potential intensification rate (PIR), similar to the MPI, can be estimated with the updated theory; and how sensitive such a PIR is to the environmental conditions and the model parameters? The rest of the paper is organized as following. Section 2 introduces the new refinements to the simple time-dependent theory that we have recently constructed (Wang et al. 2021b, 2022). In section 3, the sensitivities of the TC intensification rate and the steady-state solution (MPI) to various assumptions and parameters are discussed. Main conclusions are drawn in the last section.

2. New refinements

a. The assumed TC environment

As we mentioned in section 1, the main objective of this study is to further develop the dynamical system Eqs. (1) and (2), making it self-consistent and self-contained, so that the potential intensification rate (PIR)[1] of a TC can be determined for given favorable environmental thermodynamic conditions, similar to the commonly used theoretical MPI. The difference is in that the PIR is dependent on the intensity of the TC itself. Therefore, we first define the environmental parameters that are needed to close the dynamical system. Note that Eq. (1) can be used for both the intensification stage and the steady-state stage. In the steady state, by definition, $\partial V_m/\partial \tau = 0$ and V_m should be equal to the theoretical MPI (Emanuel 1986, 1988). In deriving Eq. (1), the air-sea enthalpy disequilibrium in Eq. (2) is defined locally under the eyewall. This means that the near surface air enthalpy under the eyewall should be given to estimate the air-sea enthalpy disequilibrium.

In Bister and Emanuel (2002), they assumed the inflow air spirals isothermally inward with a constant relative humidity (80%) along the surface layer inflow. In this case, the surface layer air enthalpy under the eyewall can be estimated using the TC environmental conditions and may is slightly higher than the surface air enthalpy in the environment because specific humidity increases slightly along the inflow as the surface air pressure decreases toward the eyewall. This can be also explained by the increase in surface air enthalpy along the boundary-layer inflow due to surface

[1] We term the intensification rate a TC can reach at a given intensity under favorable environmental conditions as the "potential intensification rate" (PIR), which is a function of TC intensity. For each TC, there exists a maximum PIR, in short MPIR, which depends on the environmental thermodynamic conditions and the assumed parameters, such as the surface exchange and drag coefficients, and is very similar to TC MPI. Since no detrimental environmental effects are considered herein, the intensification rate means the PIR in this study.

enthalpy flux. However, in reality, the downward flux of low entropy air is also common outside the eyewall of a TC due to convective downdrafts in spiral rainbands or in the outwardly tilted eyewall or convectively forced weak subsidence. This may largely offset the increase of surface air enthalpy resulting from surface enthalpy flux. Therefore, it is not unacceptable to assume that the surface air enthalpy under the eyewall is roughly equal to the surface air enthalpy in the TC environment, namely, $\kappa_b|_{r_m} \approx \kappa_{b0}$ in Eq. (2), where κ_{b0} is the surface-layer air enthalpy in the TC environment[2].

To justify the validity of the above assumption, we reexamined the full-physics axisymmetric model simulations by the cloud model (CM1, Bryan and Fritsch 2002) performed in Li et al. (2020). The ensemble simulations included different SSTs and atmospheric soundings sorted by SST over the North Atlantic and the western North Pacific. The same dataset of the model output was used to verify the theoretical time-dependent theories of TC intensification without the inclusion of dissipative heating in Wang et al. (2021a,b). We show in Fig. 1 the time-radius cross-section of the air enthalpy at the lowest model level (25 m above the sea surface) obtained from the ensemble mean of each experiment. We can see that under a wide range of SST, the air enthalpy at the lowest model level, which is used to calculate the thermodynamic disequilibrium in the numerical model, does not change much along both the radius and time. In particular, the air enthalpy near the RMW has similar values to that near the radius of 1000 km (TC environment). This indicates that the above assumption is acceptable for the simple time-dependent theory.

With the assumed $\kappa_b|_{r_m} \approx \kappa_{b0}$, if the near-surface air temperature and water vapor mixing ratio in the TC environment are T_a and q_{va0}, respectively, Eq. (2) can then be approximated as

[2] An alternative explanation of the assumption is to consider the global disequilibrium of the TC system. Namely, the enthalpy input from the underlying ocean to the TC system as a whole should include the enthalpy flux following the surface layer inflow all the way toward the eyewall. In that case, the enthalpy disequilibrium should be measured by the disequilibrium from the environment. This was arguably used to explain the existence of TC superintensity by Wang and Xu (2010), who argued that the surface enthalpy flux outside the eyewall may contribute to TC entropy budget in the eyewall and thus to partly balance the energy loss due to surface friction under the eyewall. However, in that case, the surface enthalpy flux should be estimated using the surface air pressure following the inflow air. This has not been considered in our simple theory since the surface air pressure under the eyewall is used. An equivalent assumption/approximation was also made in Emanuel (2017).

$$V_{MPI}^2 = \frac{C_k}{C_D}\varepsilon\left[c_p(T_s - T_a) + L_v\left(q_{vs}^*|_{r_m} - q_{va0}\right)\right], \tag{3}$$

where c_p is the specific heat of dry air, L_v is latent heat of vaporization, and $q_{vs}^*|_{r_m}$ is the saturation water vapor mixing ratio at SST at r_m. The saturation water vapor mixing ratio for a given SST at r_m can be given as

$$q_{vs}^* = \frac{R_d}{R_v}\frac{e_{so}}{p_m - e_{so}} = q_{vs0}^*\left(\frac{p_e - e_{so}}{p_m - e_{so}}\right), \tag{4}$$

where R_d and R_v are the gas constants of dry air and water vapor, e_{so} is the surface saturation vapor pressure at SST, p_e is the unperturbed environmental surface air pressure, p_m is the surface air pressure at r_m, and q_{vs0}^* is the surface saturation vapor mixing ratio at SST and the environmental surface air pressure, namely $q_{vs0}^* = (R_d/R_v)e_{so}/(p_e - e_{so})$.

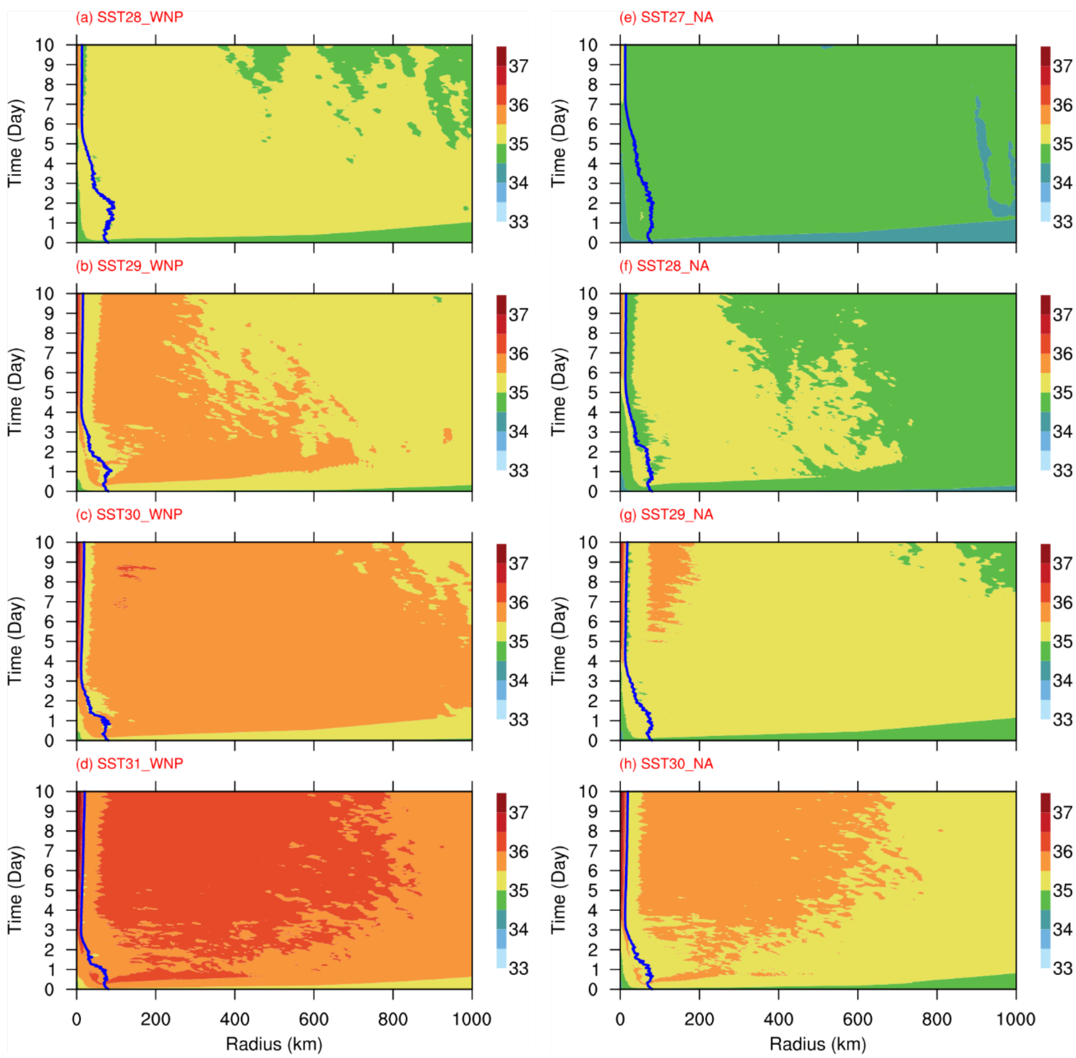

Fig. 1. The radius-time cross-section of the air enthalpy (10^4 J Kg^{-1}) at the lowest model level (25 m above the sea surface) in all experiments conducted in Li et al. (2020) for different SSTs and the corresponding SST-sorted atmospheric soundings over the western North Pacific (left) and the North Atlantic (right). The blue line indicates the radial location of the radius of maximum wind (RMW) in the corresponding experiment.

We further assume a relative humidity, RH, of the environmental near-surface air, thus we have $q_{va0} \cong RHq_{va0}^*$, where $q_{va0}^* = (R_d/R_v)e_{sa}/(p_e - e_{sa})$ is the saturation vapor mixing ratio with e_{sa} being the saturation vapor pressure at the near-surface air temperature T_a. Note that in most previous theoretical studies, the effects of air-sea temperature difference on the TC intensification rate and MPI have not been explicitly discussed (e.g., Emanuel 1986, 1988; Bister and Emanuel 2002). Using the Clausius–Clapeyron relation $[de/e = (L_v/R_v)dT/T]$, we can have the following approximation

$$q_{va0}^* = q_{vs0}^* \left[1 - \frac{L_v}{R_v T_s^2}(T_s - T_a)\right]. \tag{5}$$

With the above assumptions and approximations and considering $(p_e - e_{so})/(p_m - e_{so}) \approx p_e/p_m$, Eq. (3) can be approximated as

$$V_{MPI}^2 \approx V_{MPI0}^2 + \frac{C_k}{C_D}\varepsilon L_v q_{vs0}^* \left(\frac{p_e}{p_m} - 1\right), \tag{6}$$

where

$$V_{MPI0}^2 = \frac{C_k}{C_D}\varepsilon\left[c_p(1+\mu)(T_s - T_a) + (1 - RH)\, L_v q_{vs0}^*\right], \tag{7}$$

with $\mu = \frac{RHL_v^2 q_{vs0}^*}{c_p R_v T_s^2}$. V_{MPI0} can be considered as the MPI without considering the pressure dependence of sea surface saturation enthalpy. Because the saturation water vapor pressure is independent of air pressure, the air-sea temperature difference does not affect the pressure dependence of sea surface saturation enthalpy. Namely, the second term on the right-hand side of Eq. (6) is independent of the air-sea temperature difference. We therefore can evaluate their individual contributions to TC PIR and steady-state intensity, namely MPI, using Eq. (1) together with Eqs. (6) and (7). As we can see from Eq. (7), the term related to the air-sea temperature difference can lead to an increase in the MPI. This increase is largely contributed by the increase in the difference in the saturation vapor pressure since μ is about 2–4 under the tropical atmospheric conditions. This also means that contribution by the direct surface sensible heat flux is relatively small. This might be the reason why in most previous studies the contribution by surface sensible heat flux to TC MPI is generally considered much less important than that by surface latent heat flux.

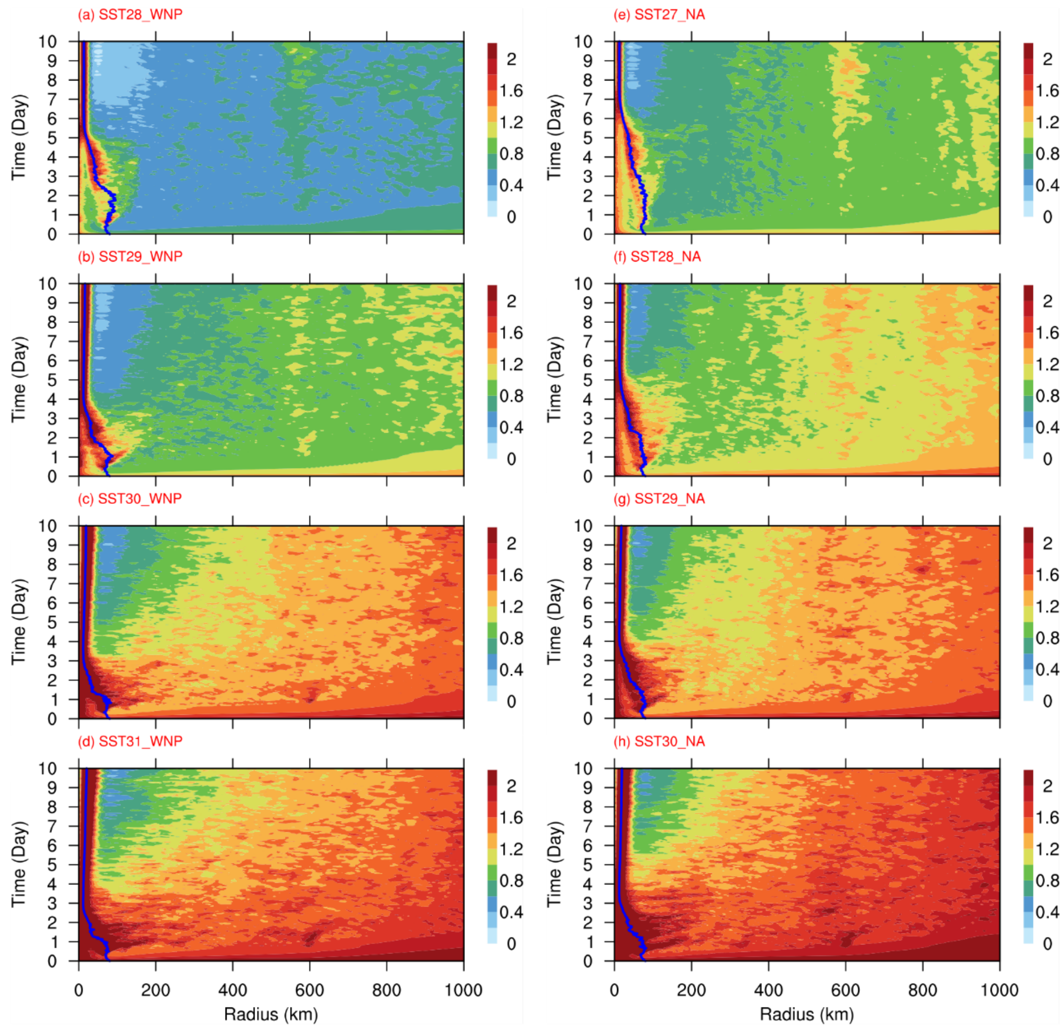

Fig. 2. As in Fig. 1 but for air-sea temperature difference (K).

To elucidate the importance of partitioning the environmental surface air enthalpy into two components, respectively, related to the air-sea temperature difference and *RH*, we show in Figs. 2 and 3 the radius-time cross-sections of air-sea temperature difference $(T_s - T_a)$ and *RH* at the lowest model level from all ensemble numerical experiments, corresponding to the surface air enthalpy shown in Fig. 1. We can see that $(T_s - T_a)$ in the TC environment (Fig. 2) shows an overall increase with increasing SST, roughly from ~0.5 K at SST=28ºC to ~1.5 K at SST=31ºC over the western North Pacific and from ~1 K from SST=27ºC to ~1.5 K at SST=30ºC over the

North Atlantic. The increase in $(T_s - T_a)$ with SST can be understood by convective activity over high SSTs where convectively unstable surface layer may produce deep well-mixed atmospheric boundary layer and ventilate the surface layer air, leading to a relatively large $(T_s - T_a)$. In contrast, over the low SSTs, the surface layer is relatively stable and air in the surface layer may keep in touch with the sea surface and less ventilated. As a result, $(T_s - T_a)$ would be relatively small over low SSTs. Different from $(T_s - T_a)$, the RH in the surface layer varies from 75% to 85%, which shows little dependence on SST (Fig. 3). As a result, the use of 80% is a good option as in previous studies (e.g., Bister and Emanuel 2002). Our results thus strongly suggest that attention needs to be given to the environmental $(T_s - T_a)$ in understanding the variability of TC MPI and intensification because the saturation air vapor pressure is a function of surface air temperature.

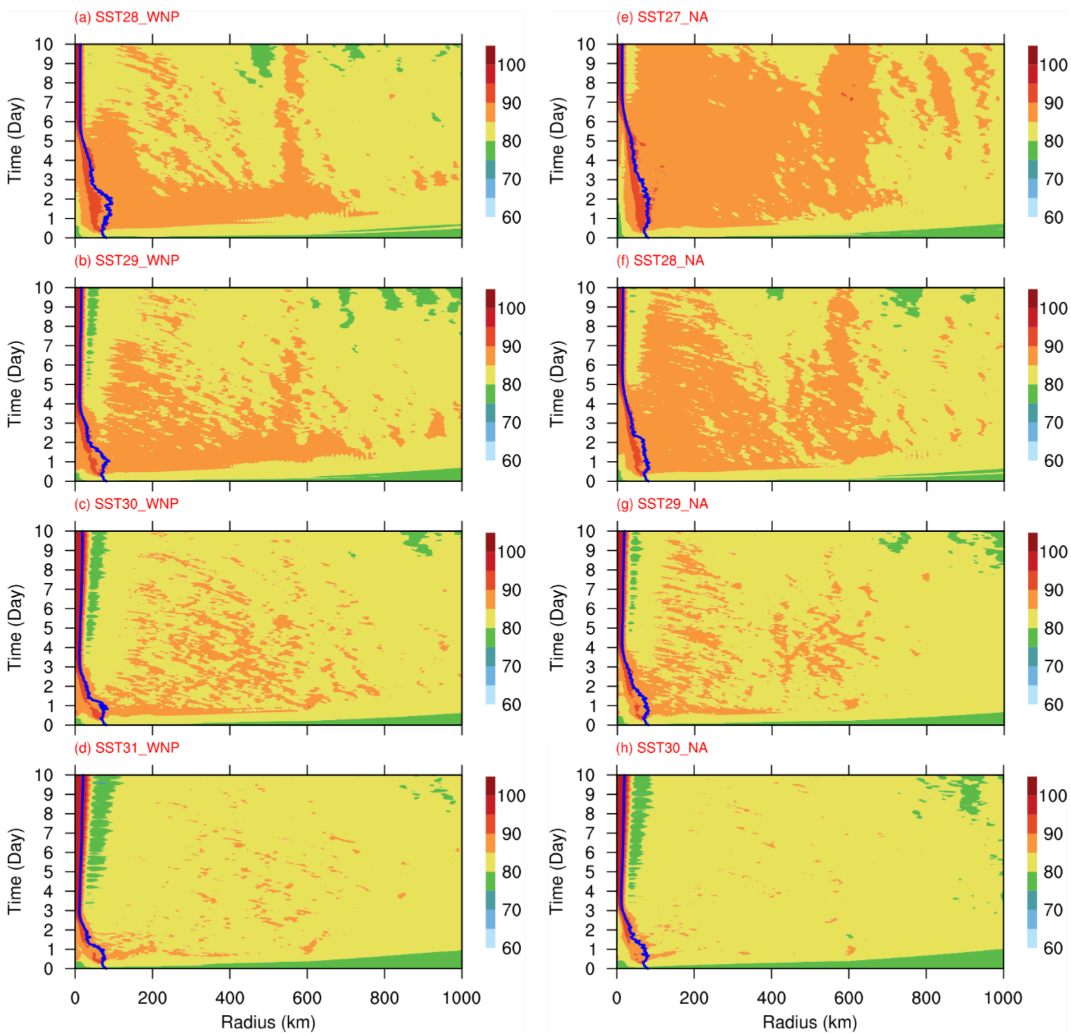

Fig. 3. As in Fig. 1 but for relative humidity (RH, %).

b. The isothermal expansion effect

Equation (1) is not closed since the surface air pressure at r_m in Eq. (6) depends on real-time TC intensity (namely V_m). Such a dependence is often termed "isothermal expansion effect". To include this effect, we first assume that the tangential wind (V) inside the RMW follows the cyclostrophic wind balance, namely

$$\alpha_d \frac{\partial p}{\partial r} = \frac{V^2}{r}, \quad (8)$$

where p is air pressure, $\alpha_d = R_d T_s / p$ is specific volume of dry air. We further assume that the tangential wind inside the RMW follows the following radial distribution (see also Emanuel 1995)

$$V = V_m \left(\frac{r}{r_m}\right)^b, \quad (9)$$

where b (> 0) is an empirical constant determining the radial distribution of tangential wind inside the RMW. If $b = 1$, the motion inside the RMW will be in solid-body rotation. Substituting Eq. (9) into Eq. (8) and integrating the resultant cyclostrophic wind equation from $r = 0$ to $r = r_m$, we get

$$ln\left(\frac{p_m}{p_c}\right) = \frac{V_m^2}{2bR_d T_s}, \quad (10)$$

where p_c is the surface air pressure at the TC center. Since $(p_m - p_c) \ll p_c$, Eq. (10) can be approximated as

$$\frac{p_m}{p_c} - 1 \approx \frac{V_m^2}{2bR_d T_s}. \quad (11)$$

Although p_c and p_m are both unknown, they are not independent of each other. To find out an approximate relationship between p_c and p_m, we reanalyzed the results from the ensemble simulations by Li et al. (2020). Figure 4a shows the scatter plots of $p_e/p_m - 1$ against $p_m/p_c - 1$ from all ensemble simulations. From Fig. 4a, we can find a nearly linear relationship between the two quantities given below.

$$\frac{p_e}{p_m} - 1 \cong c'\left(\frac{p_m}{p_c} - 1\right), \quad (12)$$

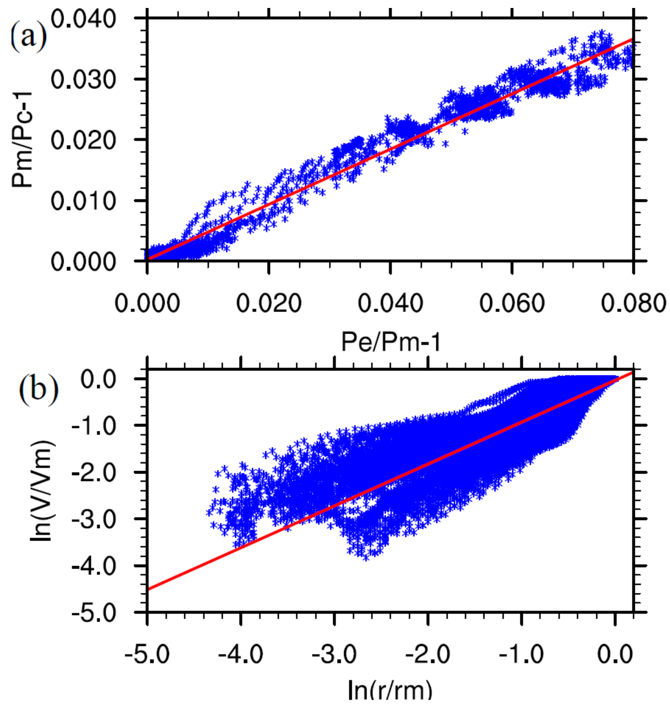

Fig. 4. The scatter plots of (a) $p_e/p_m - 1$ against $p_m/p_c - 1$ and (b) $ln(r/r_m)$ against $ln(V/V_m)$ based on results from the ensemble simulations using the axisymmetric full-physics cloud model CM1 with different SSTs and atmospheric soundings sorted by SST under TC conditions over the North Atlantic and the western North Pacific (see Li et al. 2020 for details of the model simulations). The red line indicates the best linear fitting.

where *c'* is a nondimensional parameter, which is ~2.0 as we can see from Fig. 4a. Note that *c'* may be subject to some variability if different initial vortex structures are used in model simulations or with different model simulations or different environmental conditions. Our preliminary results indicate that *c'* varies mostly between 1.5–2.0 (not shown), and thus we consider it as an empirical parameter with some small uncertainties. With Eqs. (11) and (12), Eq. (6) can be reduced to

$$V_{MPI}^2 \approx V_{MPI0}^2 + \kappa V_m^2, \tag{13}$$

where

$$\kappa = \frac{C_k}{C_D} \varepsilon \frac{c L_v q_{vs0}^*}{2 R_d T_s}, \tag{14}$$

with $c = c'/b$. Note that c' and b are often not independent, while the parameter c can be considered as an empirical parameter independent of the TC intensity. Our diagnostics based on the ensemble simulations shows that b is around 0.9 (Fig. 4b). Therefore, in the calculations below, we subjectively assume $c = 2.0$. From Eq. (14), assuming $\kappa = 0.0$ is equivalent to ignoring the pressure dependence of surface saturation enthalpy. In that case, the second term on the right-hand side of Eq. (6) or Eq. (13) becomes zero.

An alternative approach to the derivation of an approximate relationship between the surface air pressure under the eyewall and the maximum wind speed can be found in Emanuel (2017). He assumed the boundary layer flow being steady and frictionless and integrated the Bernoulli equation from the environment, where $p = p_e$ and $V = 0$, to r_m, where $p = p_m$ and $V = V_m$

$$\int_e^{r_m} \frac{dp}{\rho} = \int_e^{r_m} R_d T_s d(lnp) = R_d T_s ln\left(\frac{p_m}{p_e}\right) = -\frac{1}{2} V_m^2. \tag{15}$$

An approximate relationship between V_m and surface air pressure at r_m from Eq. (15) can be given below

$$\frac{p_e}{p_m} - 1 \cong \frac{1}{2} \frac{V_m^2}{R_d T_s}. \tag{16}$$

With the above approximation, the parameter κ in Eq. (14) will be replaced by k' given below

$$k' = \frac{C_k}{C_D} \varepsilon \frac{L_v q_{vs0}^*}{2R_d T_s}. \tag{17}$$

The difference between Eq. (17) with Eq. (14) lies in a factor of c in the former. Since $c \approx 2.0$, we can see that the use of Eq. (17) may underestimate the isothermal expansion effect by 50% on the MPI and thus Eq. (17) can only give a conservative estimation of the isothermal expansion effect. Note also that Eq. (17) is based on the Bernoulli principle with the assumptions of steady and frictionless flow. However, the boundary layer in an intensifying TC is not steady and with strong surface friction.

With the approximation Eq. (14), Eq. (1) can be rewritten as

$$\frac{\partial V_m}{\partial \tau} = \frac{\alpha C_D}{h} \left\{ A V_{MPI0}^2 - \left[1 - A\kappa - \gamma A \varepsilon \left(1 - \frac{\delta C_k}{2C_D}\right)\right] V_m^2 \right\}. \tag{18}$$

As in Wang et al. (2022), we take the parameter A to be a function of the relative intensity given below

$$A = \left(\frac{V_m}{V_{maxt}}\right)^{3/2}, \tag{19}$$

where V_{maxt} can be considered as the time-dependent MPI with the effect of dissipative heating at the current TC intensity (Wang et al. 2022) and is defined below

$$V_{maxt} = \sqrt{V_{MPI0}^2 + A\left[\kappa + \gamma\varepsilon\left(1 - \frac{\delta C_k}{2C_D}\right)\right]V_m^2}. \quad (20)$$

Since V_{maxt} is a function of A for a given V_m, Eqs. (19) and (20) can be solved iteratively to get A (often three iterations are accurate enough). We can see from Eq. (20) that V_{maxt} is close to V_{MPI0} at the weak stage of the TC because both the isothermal expansion effect and dissipative heating are relatively small when the TC is weak, but it increases as the TC intensifies. Once the TC reaches its steady state, A approaches 1.0. Note that the parameter A can be modified to partially depend on the TC inner-core size via the inertial stability (Wang et al., 2021a). In that case, the functional relationship between A and the relative intensity should be modified (Wang et al. 2021a,b). Nevertheless, in our latest version of the theoretical model, no explicit TC structure parameter is included. This can be explained by the fact that part of the structure dependence of TC intensification can be reflected in the TC intensity dependence as advocated by Wang et al. (2021b).

c. The outflow temperature

Given the SST, the boundary-layer RH and air-sea temperature difference in the TC environment, the assumed constant c, and the ratio of exchange and drag coefficients, we still need to know the outflow-layer air temperature T_o to estimate the thermodynamic efficiency ε. Although T_o varies with the TC intensification (Emanuel 2012), it is largely determined by the environmental atmospheric sounding for the corresponding SST. Previous studies show that the outflow-layer air temperature is not independent of the corresponding SST (e.g., Zeng et al. 2008). Following Zeng et al. (2008), we approximate T_o as the air temperature near the tropopause, namely the minimum temperature where the lapse rate changes from negative to positive value with height. To establish a relationship between T_o and T_s, we estimated T_0 for all TC cases during 1999–2019 over the North Atlantic based on the interim reanalysis data from the European Centre for Medium-Range Weather Forecasting (ERA-Interim; Dee et al. 2011). The extended best-track (EBT) dataset (Demuth et al. 2006) at 6-h interval is used to track all TCs with maximum sustained wind speed greater than 18 m s^{-1}. The dataset was updated in March 2021 (version 3.0.0) using all data available in the National Hurricane Center Best Track Data (HURDAT2, Landsea and Franklin 2013).

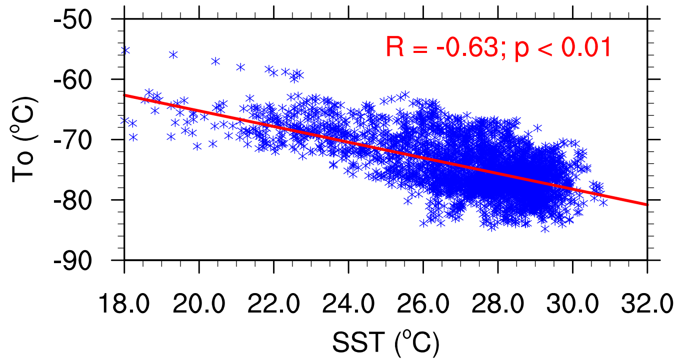

Fig. 5. Scatter plots of the outflow-layer air temperature (T_o, °C) against SST (°C) and the fitted curve (red) for all TC cases during 1999–2019 over the North Atlantic based on the ERA-Interim data. R is the linear correlation coefficient with p-value less than 0.01, namely significant at 99% confidence level.

Figure 5 shows the scatter plots of the estimated outflow-layer air temperature against the corresponding SST for all TC cases during 1999–2019 over the North Atlantic. Similar to the results of Zeng et al. (2008), the outflow-layer air temperature obtained in such a way decreases with increasing SST. This implies that the thermodynamic efficiency increases as SST increases (see also Fig. 2b in Zeng et al. 2008). The best fitted curve for the dependence of T_o on T_s for all data points shows a linear relationship given below

$$T_o = 233.9 - 1.3 \times (T_s - 273.15). \tag{21}$$

Although considerable variability for any given SST exits, over 85% of the outflow-layer air temperatures vary between -5 K and +5 K about the fitted line. The effect of such variability on the calculated ε and thus the MPI are generally moderate (not shown), indicating weak dependence of ε on the outflow-layer air temperature. We note that although the use of the lower outflow-layer temperature for a given SST may give the higher potential intensification rate and steady-state intensity, the difference between those calculated using the best-fitted and the lowest outflow-layer temperature for a given SST is generally in several percentages (not shown). Because of the simplicity of the theoretical model, the small change due to the outflow-layer temperature uncertainty is acceptable. It should be mentioned that the relationship Eq. (21) is fitted based on current climate. The extrapolation of T_o to higher SST, for example, that induced by global warming should be with caution. Nevertheless, it is possible to construct a new relationship between T_o and T_s for future climate based on projections from high-resolution climate simulations, which is beyond the scope of this work but is a good topic for a future study.

The time-dependent Eq. (18) with Eqs. (19)–(21) can then be used to evaluate contributions of the pressure dependence of surface saturation enthalpy (namely the isothermal expansion effect), the air-sea temperature difference, and the boundary layer relative humidity in the TC environment on both the TC PIR and the steady-state intensity (MPI) with and without the inclusion of dissipative heating for a given SST. It can also be used to examine the sensitivity of the corresponding TC PIR and MPI to various parameters, such as the surface exchange and drag coefficients. These will be discussed in the next section.

3. The model sensitivity

a. The steady- state solution

We first discuss the steady-state solution of Eq. (18), namely the MPI. In this case, we have $\frac{\partial V_m}{\partial \tau} = 0$ and $A = 1.0$, the MPI from Eq. (18) can be expressed as

$$V_{MPI}^2 = \frac{V_{MPI0}^2}{1-\kappa-\gamma\varepsilon\left(1-\frac{\delta C_k}{2C_D}\right)}. \qquad (22)$$

Figure 6 shows the dependence of the calculated MPI on SST in three different cases. The first (black) is the control with ($V_{MPI0} + IE$, solid) and without (V_{MPI0}, dashed) considering the pressure dependence of sea surface saturation enthalpy (namely the isothermal expansion effect). The second (red) is the same as the control but with dissipative heating included (DH). In both the first and second cases, a zero environmental air-sea temperature difference is assumed (T_a=SST). The third (green) is the same as the second case but with 1°C air-sea temperature difference (V_{MPI0}+DH+dT=1C). In these calculations, we assumed $c = 2.0$ (Figs. 4a,b), $C_k = 1.2 \times 10^{-3}$, $C_D = 2.4 \times 10^{-3}$, $\delta = 1.0$, the environmental sea surface pressure $p_e = 1010\ hPa$, and a boundary layer $RH = 80\%$ in the TC environment. In addition, we used $\gamma = 0.8$ in Eq. (22) for the case including dissipative heating due to surface friction, which is based on the theoretical consideration by Kieu (2015) and the recent evaluation of the same framework using observations in Wang et al. (2022).

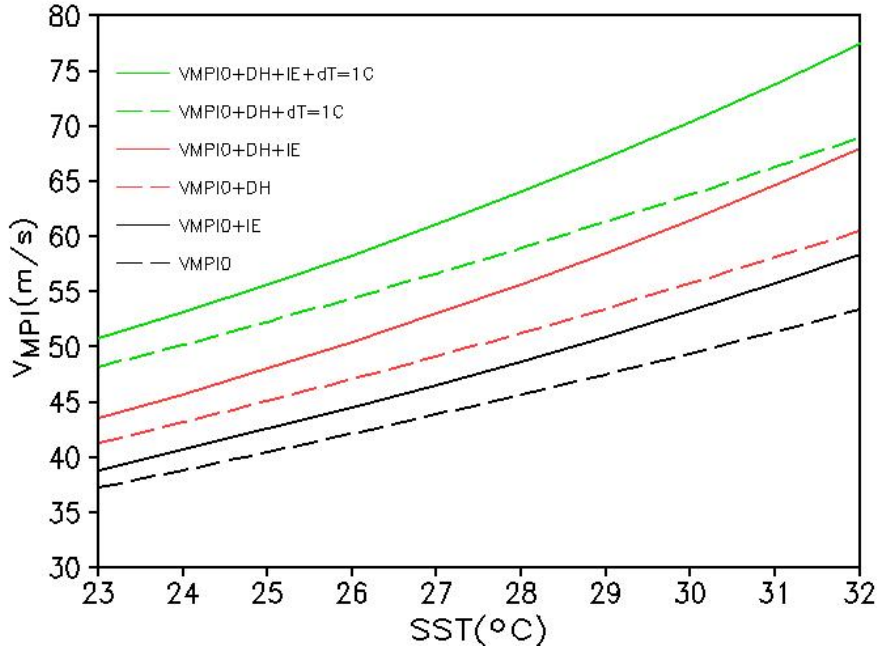

Fig. 6. The MPIs (V_{MPI}, m s^{-1}) as a function of SST (^{o}C) for three cases: without considering dissipative heating (black, $\gamma = 0$), with dissipative heating (red, $\gamma = 0.8$), and with 1^{o}C of air-sea temperature difference (dT=1C, green). The solid curves correspond to solutions with the isothermal expansion (IE) effect included while the dashed curves correspond to solutions without the isothermal expansion effect ($\kappa = 0$). In these calculations, $c = 2.0$, $C_k = 1.2 \times 10^{-3}$, $C_D = 2.4 \times 10^{-3}$, $\delta = 1.0$, $p_e = 1010\ hPa$, and $RH = 80\%$ are used.

We can see several interesting features from Fig. 6. First, the MPI increases with increasing SST in all three cases. Second, the dependence of MPI on the isothermal expansion increases with increasing SST and the increase in the MPI itself. Third, the increase in MPI due to dissipative heating is about twice as large as that induced by the isothermal expansion effect and also increases with increasing SST or the MPI as the isothermal expansion effect. This is mainly because both the sea saturation enthalpy and dissipative heating increase with increasing SST (and MPI). Fourth, the air-sea temperature difference can lead to an increase in the MPI comparable to the effect of dissipative heating, which is almost independent of SST or the MPI itself. Surprisingly, the increase in the MPI due to the increase of 1^{o}C in the air-sea temperature difference is comparable to that induced by 3^{o}C increase in SST. Note that most previous studies indicate the importance of environmental relative humidity and SST to the MPI (e.g., Emanuel 1988). Our results demonstrate that the air-sea temperature difference is another important environmental factor that can greatly contribute to TC MPI. This large effect is mainly due to the reduced saturation vapor pressure of surface air and thus the increased moisture disequilibrium at the air-sea interface for a given boundary-layer relative humidity in the TC environment.

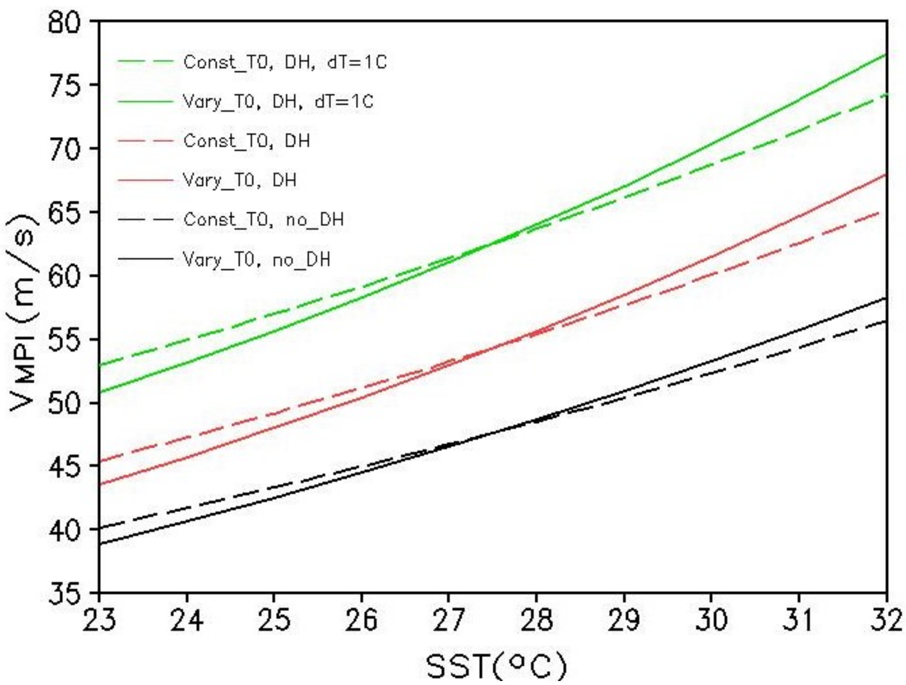

Fig. 7. The solid curves are the same as those in Fig. 6 and the dashed curves correspond to the results with the outflow-layer air temperature independent of SST and equals to the corresponding value at SST=27.5°C.

Since large variability exits in the outflow-layer air temperature (Fig. 5), it is our interest to further examine how sensitive the MPI is to the change in the outflow-layer air temperature. For this purpose, we compare in Fig. 7 the MPIs for three cases with the isothermal expansion effect (solid, as shown in Fig. 6) and those with the outflow-layer air temperature fixed at the value corresponding to SST=27.5°C (dashed). As expected, the lower outflow-layer air temperature contributes positively to the MPI. This effect increases slightly with the increase in the MPI itself because of the increasing effect of dissipative heating. Nevertheless, changes due to the increase/decrease in the outflow-layer air temperature are often moderate compared with the isothermal expansion effect, the effect of dissipative heating, and the environmental air-sea temperature difference. This suggests that the fitted dependence of the outflow-layer air temperature as a function of SST given in Eq. (21) can be used to estimate the outflow-layer air temperature as a good approximation and thus the MPI. We noticed that in a recent theoretical framework, Rousseau-Rizzi and Emanuel (2021) assumed the weak temperature gradient (WTG) with the outflow layer temperature being independent of local SST. In that case, not only the possible dependence of the outflow layer temperature on local SST but also the possible effect of the variability of the outflow temperature on TC MPI are ignored. We choose to use the fitted dependence of the outflow-layer temperature on SST.

b. The intensification rate

We first examine the intensification rate, namely PIR, as a function of relative intensity defined as the intensity normalized by the corresponding MPI for a given SST under four conditions (Fig. 8). The first is the control under which neither the isothermal expansion effect nor the dissipative heating is considered. The second is the same as the control but with the isothermal expansion effect considered. The third is the same as the control but with the dissipative heating included. The fourth is the same as the control by with both the isothermal expansion effect and dissipative heating considered. Two calculations are done for each condition: one with zero air-sea temperature difference and one with the surface air temperature being 1^{o}C lower than the underlying SST in the TC environment. Consistent with the findings in Wang et al. (2022), the inclusion of dissipative heating leads to an increase in intensification rate and a slight shift of the maximum intensification rate (namely MPIR) towards the higher relative intensity side. The isothermal expansion shows a similar effect but leads to an increase in intensification rate by about half of that induced by dissipative heating. This is consistent with the effects of isothermal expansion and dissipative heating on the MPI as shown in Fig. 6. The 1^{o}C air-sea temperature difference in the environment leads to an increase in the maximum intensification rate similar to that induced by dissipative heating. This demonstrates that the environmental air-sea temperature difference is another important factor that can considerably enhance the TC intensification rate and MPI.

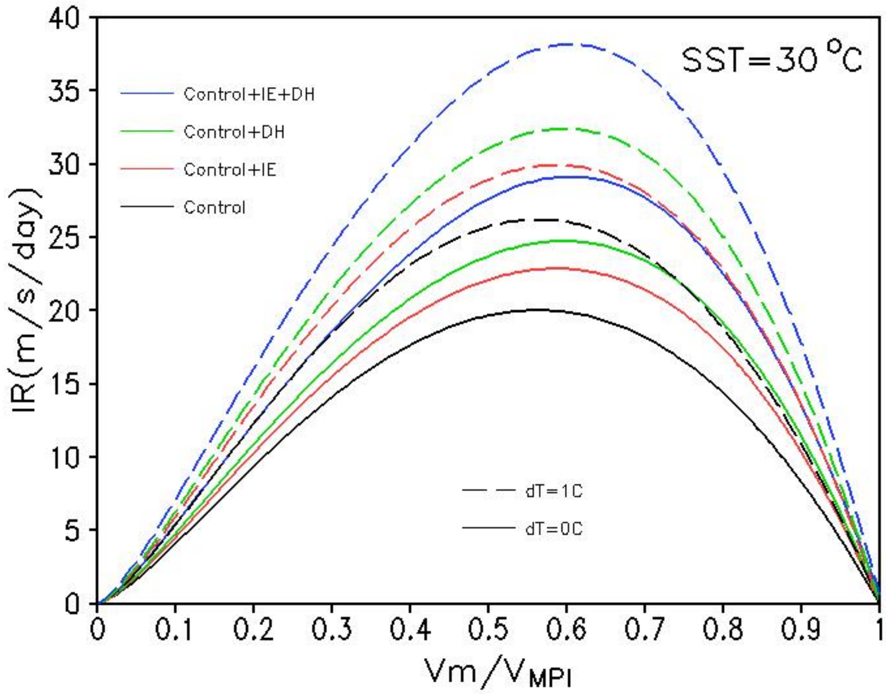

Fig. 8. Intensification rate (IR, m s^{-1} day^{-1}) as a function of relative intensity (intensity normalized by the corresponding MPI) for a given SST of 30°C under four conditions, including the control (Control, black) without considering the effect of either isothermal expansion or dissipative heating, that as the control but with the isothermal effect included (Control+IE, red), that as the control but with dissipative heating included (Control+DH, green), and that as the control but with both isothermal expansion and dissipative heating included (Control+IE+DH, blue). Solid curves are for results with zero environmental air-sea temperature difference (dT=0C) and dashed curves are for those with 1°C environmental air-sea temperature difference (dT=1C).

We can also see from Fig. 8 that the intensification rate reaches a maximum near the relative intensity of 0.6 in the case with both isothermal expansion effect and dissipative heating. We now examine the sensitivities of the maximum intensification rate to the surface drag and exchange coefficients with the results shown in Fig. 9. The maximum intensification rate increases almost linearly with increasing surface exchange coefficient (dashed curve in Fig. 9) while it is insensitive to surface drag coefficient although a very weak decreasing trend is visible (solid curve in Fig. 9). Note that the MPI is proportional to the square root of the ratio of surface exchange to drag coefficients as we can see from Eq. (7), while the intensification rate is proportional to the square of the MPI (Wang et al. 2021a,b, 2022). As a result, given a drag coefficient and relative intensity, the (maximum) intensification rate would increase about linearly with surface exchange coefficient as we can see from Fig. 9. Although Eq. (18) shows a proportion of the intensification rate to surface drag coefficient, the increase in drag coefficient reduces the MPI. The two effects are compensated, resulting in little difference in the maximum intensification rate for the drag coefficient in reasonable range. This is also supported by results of Li and Wang (2021a), who found that the intensification rate of a numerically simulated TC is insensitive to surface drag coefficient during the primary intensification stage. We will show below that some sensitivity to surface drag coefficient occurs at the weak intensity stage of a TC, which is also consistent with previous numerical simulations using full-physics models (Kilroy et al. 2017; Li and Wang 2021a).

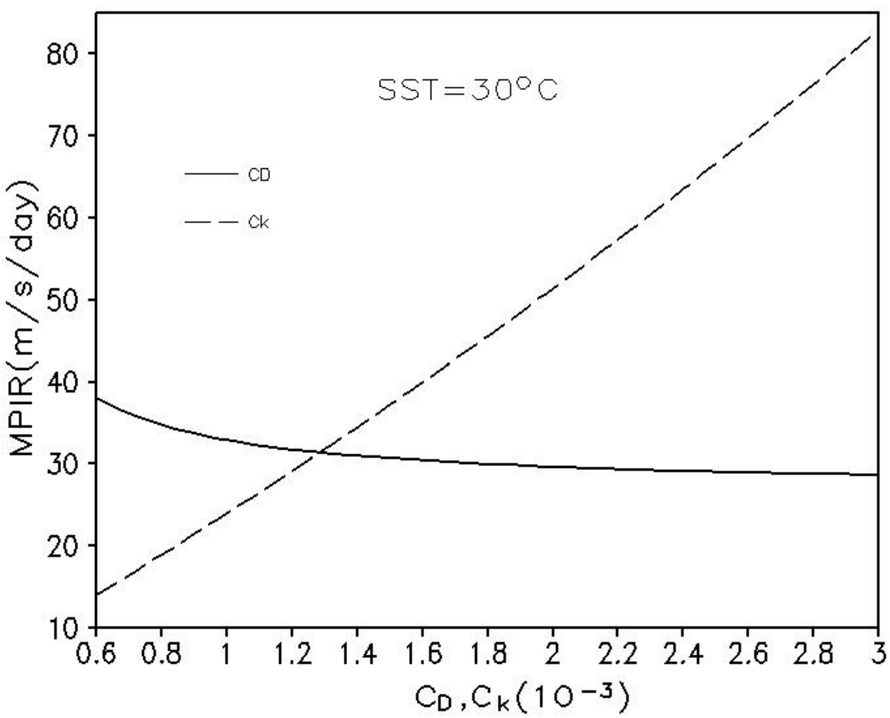

Fig. 9. The maximum (potential) intensification rate (MPIR, m s^{-1} day^{-1}) as a function of drag coefficient (C_D, solid) and enthalpy exchange coefficient (C_k, dashed) for given SST=30°C with both isothermal and dissipative heating included and the same other parameters as used in Fig. 6.

The sensitivities of the maximum intensification rate to the three environmental parameters, namely SST, boundary-layer *RH*, and air-sea temperature difference in the TC environment are also examined. We first look at the dependence of the maximum intensification rate on SST (black, Fig. 10). For given surface drag and exchange coefficients, the maximum intensification rate increases with increasing SST almost exponentially. This is expected since the intensification rate is proportional to sea surface saturation enthalpy, which is an exponential function of SST as implied by the Clausius–Clapeyron relation. For a given SST, the increase in the environmental boundary-layer *RH* leads to a nearly linear decrease in the maximum intensification rate (red, Fig. 10), which also leads to a decrease in the MPI (not shown). This occurs because the intensification rate is negatively correlated with the environmental boundary-layer *RH* as implied from Eqs. (7) and (18).

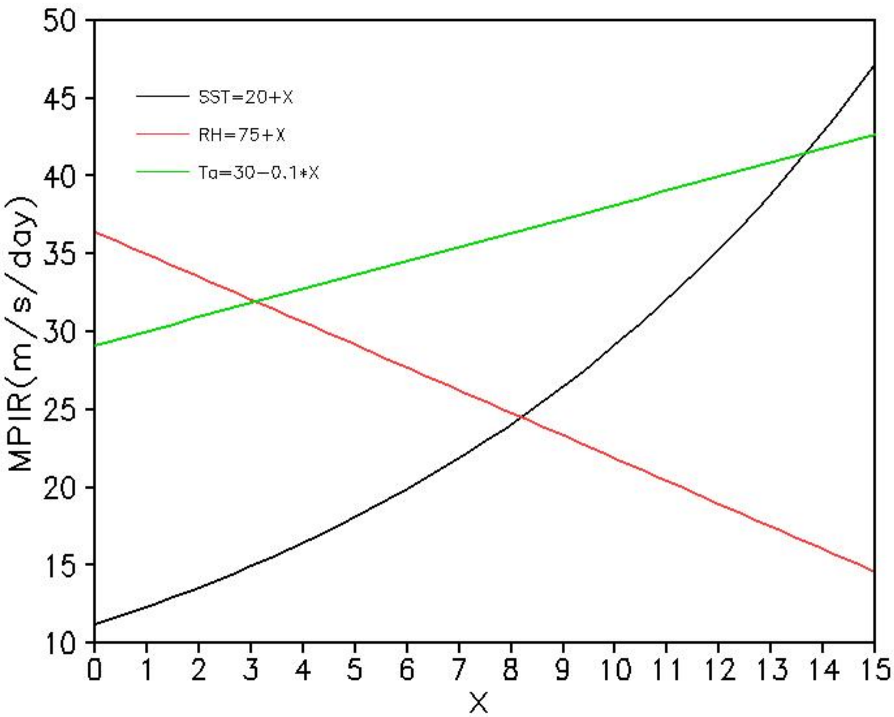

Fig. 10. The maximum (potential) intensification rate (MPIR, m s^{-1} day^{-1}) as a function of SST (20+X°C, black) for a given *RH*=80% and zero environmental air-sea temperature difference, a function of the environmental *RH* (75+x%, red) for SST=30°C and zero environmental air-sea temperature difference, and a function of the environmental air-sea temperature difference (Ta=30-0.1X°C), green) for SST=30°C and *RH*=80%. In all calculations, both isothermal and dissipative heating are included and all other parameters are the same as those used in Fig. 6.

Note that although the environmental boundary-layer *RH* is important to convection during TC genesis stage, higher environmental *RH* is unfavorable for TC rapid intensification, which often occurs at intermediate TC intensity (Xu and Wang 2015, 2018a; Xu et al. 2016). In contrast, an increase in the environmental air-sea temperature difference leads to a nearly linear increase in the maximum intensification rate (green, Fig. 10). The increase in environmental air-sea temperature difference also leads to a considerable increase in the MPI (Fig. 6). The nearly linear increase in the maximum intensification rate with increasing environmental air-sea temperature difference can be seen clearly from Eqs. (7) and (18). This increase is largely due to the dependence of surface vapor saturation pressure on the near-surface air temperature for a given environmental *RH* under the mean tropical conditions.

c. The time-dependent solution

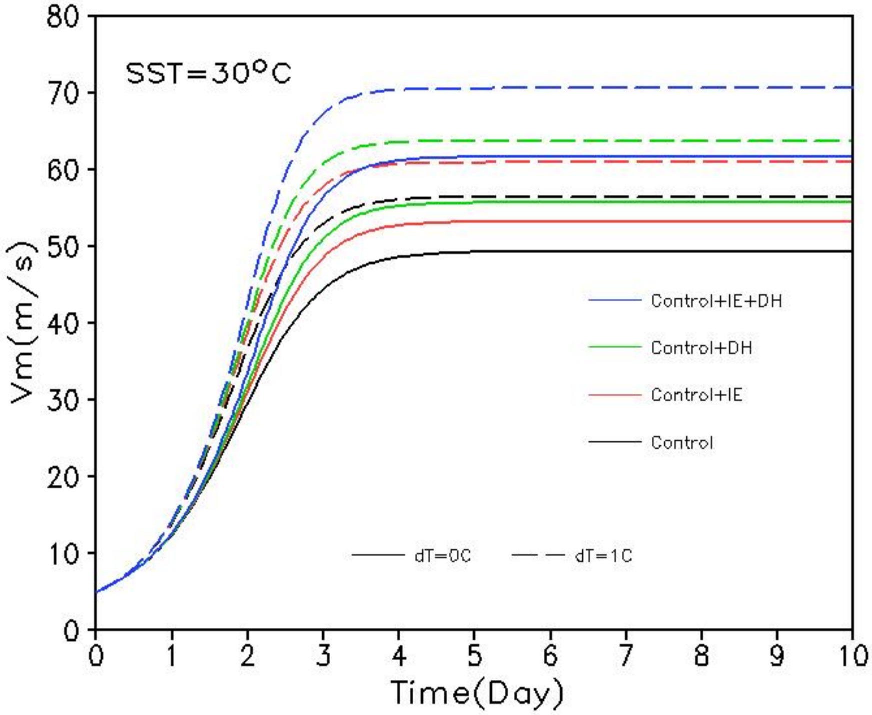

Fig. 11. Time-dependent solutions of TC intensity (V_m, m s^{-1}) obtained by time-integration of Eq. (18) with the use of Eqs. (19) and (20) for a given SST of 30°C with the initial V_m of 5 m s^{-1} under four conditions as in Fig. 8, including the control (Control, black) without considering the effect of either isothermal expansion or dissipative heating, that as the control but with the isothermal expansion effect included (Control+IE, red), that as the control but with dissipative heating included (Control+DH, green), and that as the control but with both isothermal expansion and dissipative heating included (Control+IE+DH, blue). Solid curves are for results with zero environmental air-sea temperature difference (dT=0C) and dashed curves are for those with 1°C environmental air-sea temperature difference (dT=1C). Other parameters are the same as those used in Fig. 6.

Now we give some examples of the time-dependent solution of Eq. (18) obtained by the simple leap-frog scheme with the Asselin time filter (Asselin 1972). Figure 11 shows the time-dependent solutions with various assumptions, including the basic solution without considering the effect of isothermal expansion effect or dissipative heating and those with and without the environmental air-sea temperature difference. Consistent with the results shown in Figs. 6 and 8, both the intensification rate and the steady-state intensity of the TC increase with the inclusion of either the isothermal expansion effect or dissipative heating or both. The isothermal expansion imposes an overall effect on both the intensification rate and steady-state intensity about half of that induced by dissipative heating. Their effects are almost linear and additive as implied by Eqs. (18) and (22). It is shown that 1°C environmental air-sea temperature difference leads to an increase in both the intensification rate and the steady-state intensity comparable to the inclusion of dissipative heating. We also found that assuming a zero environmental air-sea temperature difference often underestimates the observed maximum TC intensity (not shown), which is supported by the studies of Xu et al. (2019a,b).

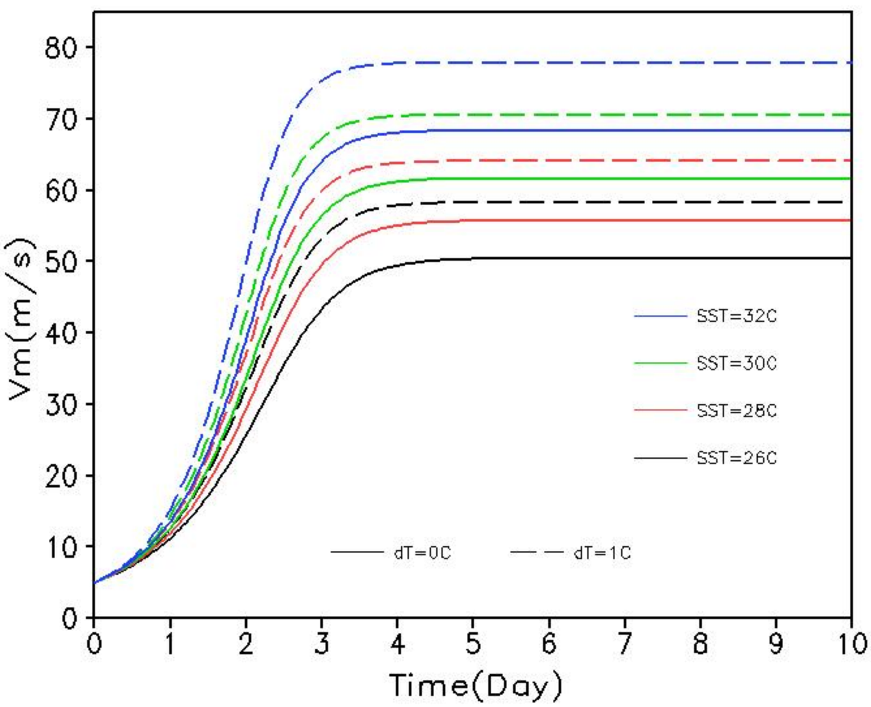

Fig. 12. Time-dependent solutions of TC intensity (V_m, m s^{-1}) obtained by time-integration of Eq. (18) with the use of Eqs. (19) and (20) for different SSTs with the initial V_m of 5 m s^{-1} for two cases: one with zero environmental air-sea temperature difference (dT=0, solid) and one with 1°C environmental air-sea temperature difference (dT=1C, dashed). In these calculations, both the isothermal expansion and dissipative heating are included and all other parameters are the same as those used in Fig. 6.

Although both the intensification rate and the steady-state intensity increase with increasing SST and the environmental air-sea temperature difference (Fig. 12), 1°C increase in SST leads to only 5% increase in the MPI and the intensification rate, while 1°C increase in the environmental air-sea temperature difference leads to an increase of about 15% in both. Namely, 1°C change in environmental air-sea temperature difference can result in a threefold change in both the TC intensification rate and MPI induced by 1°C change in SST. This further demonstrates the importance of the environmental air-sea temperature difference to TC intensification and maximum intensity. Note that this dramatic effect of environmental air-sea temperature difference on TC intensification and MPI has not been explicitly/quantitatively discussed in previous time-dependent theories although air-sea temperature difference exists in general in the tropics (Xu et al. 2019a,b).

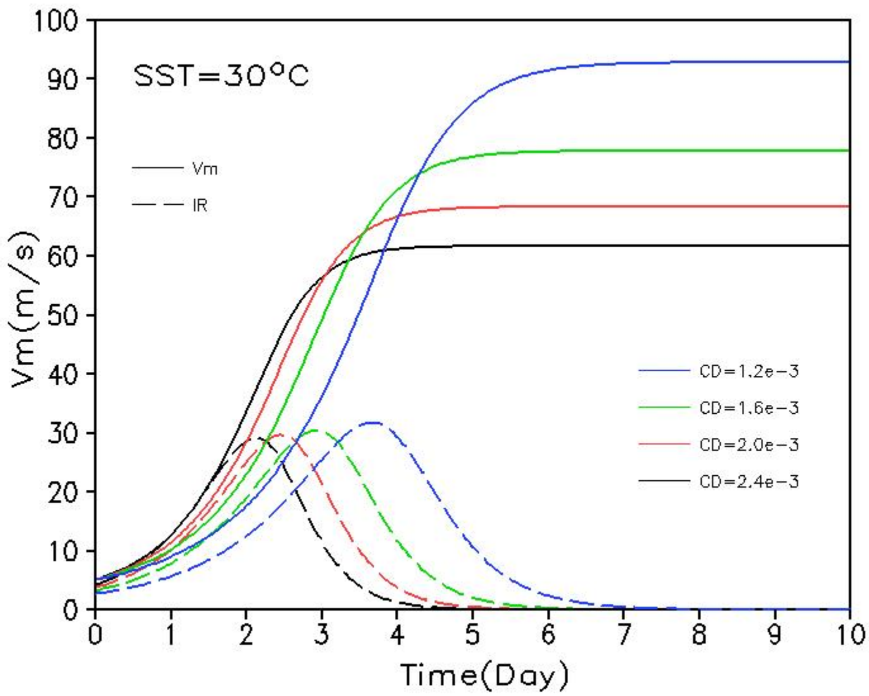

Fig. 13. Time-dependent solutions of TC intensity (V_m, m s^{-1}, solid) obtained by time-integration of Eq. (18) with the use of Eqs. (19) and (20) for a given SST=30°C with the initial V_m of 5 m s^{-1} and zero environmental air-sea temperature difference using different surface drag coefficients. The dashed curves are the corresponding intensification rate (m s^{-1} day^{-1}). In these calculations, both the isothermal expansion and dissipative heating are included and all other parameters are the same as those used in Fig. 6.

Finally, we examine the sensitivity of the time-dependent solution to surface drag coefficient. We can see from Fig. 13 that the maximum intensification rate depends very weakly on surface drag coefficient (dashed, Fig. 13) as shown in Fig. 9, and the steady-state intensity decreases with increasing surface drag coefficient as inferred from the MPI given in Eqs. (7) and (22). However, larger surface drag coefficient leads to earlier intensification of the TC (solid, Fig. 13). This is mainly because the parameter A is a function of the relative intensity defined in Eq. (19). Larger surface drag coefficient reduces the MPI, and thus, for the same intensity, a reduced MPI indicates a higher relative intensity, and a larger parameter A. This can also be explained as a result of the increasing boundary-layer mass convergence and the contraction of the RMW as surface drag coefficient increases in the early stage of TC intensification. This would lead to a tendency of increasing the degree of congruence between the moist entropy surface and absolute angular momentum surface in the eyewall updraft (Wang et al. 2021b) or a tendency of increasing inner-core inertial stability and the dynamical efficiency of eyewall heating (Wang et al. 2021a). Similar sensitivity has also been found in full-physics model simulations in previous studies (e.g., Kilroy et al. 2017; Li and Wang 2021a). However, we found that such a sensitivity depends strongly on TC intensity and only obvious when the TC is in the weak intensity stage. This is confirmed by the time-dependent solution with the initially TC intensity of 17.2 m s^{-1} shown in Fig. 14. This demonstrates that for a TC after reaching the tropical storm intensity, its intensification rate becomes insensitive to surface drag coefficient. This agrees with previous full-physics model simulations (e.g., Peng et al. 2018; Li and Wang 2021a).

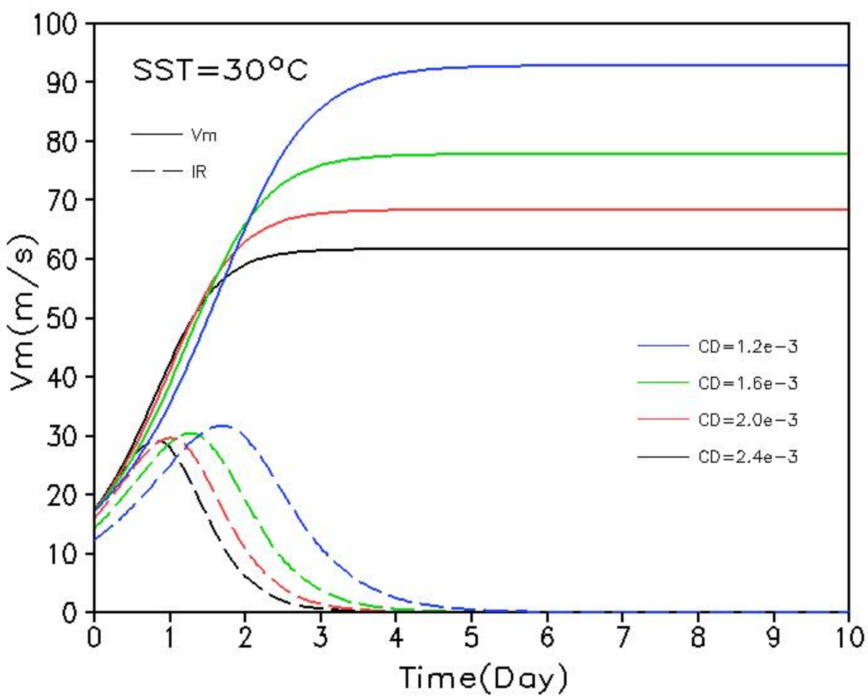

Fig. 14. As in Fig. 13 but with the initial V_m of 17.2 m s^{-1}, namely the tropical storm intensity.

4. Conclusions and discussion

In the last decade or so, several efforts have been devoted to the development of time-dependent theories of TC intensification, which can help quantify TC intensification based on a simplified dynamical system model (Emanuel 2012; Ozawa and Shimokawa 2015; Wang et al. 2021a,b, 2022). A key unresolved issue in the current theories developed so far is the lack of a closure required to take into account of the pressure dependence of sea surface saturation enthalpy, namely the isothermal expansion effect, under the eyewall. Two other issues are the definitions of the TC environment and the outflow-layer air temperature. In this study, a closure has been developed for the time-dependent theory of TC intensification most recently updated with the inclusion of dissipative heating by Wang et al. (2022). A key to the closure is to find a functional relationship between the surface air pressure under the eyewall and the TC intensity. This is achieved based on the cyclostrophic wind balance and calibrated using full-physics cloud-resolving model simulations. Although the outflow-layer air temperature is often considered as an environmental parameter, it is highly and negatively correlated with the underlying SST. Based on global reanalysis data, a linear relationship between the outflow-layer air temperature and SST is also constructed. As a result, given the environmental thermodynamic conditions, including the boundary-layer relative humidity and surface air-sea temperature difference in the TC environment, and the assumed surface drag and exchange coefficients, the time-dependent theory with the refinements documented in this study can give the intensity-dependent intensification rate and the steady-state TC maximum intensity. Namely, with the refinements, the updated simple time-dependent theory of TC intensification becomes self-contained and is more practical.

It is shown that under the mean tropical conditions the pressure dependence of sea surface saturation enthalpy can lead to an increase in both the steady-state TC intensity, namely the MPI, and the intensification rate about 50% of that induced by dissipative heating due to surface friction. Results from sensitivity calculations and time-dependent numerical solutions show that both the MPI and intensification rate increase with increasing SST, surface exchange coefficient, and the environmental air-sea temperature difference, but decrease with increasing the environmental boundary-layer relative humidity. Results also show the significant contribution of the environmental near-surface air-sea temperature difference to both the TC intensification rate and MPI. We found that 1ºC increase in the environmental air-sea temperature difference can lead to an increase in both the MPI and the intensification rate comparable to that induced by dissipative heating or by an increase of 3ºC in SST. Another interesting result is the negligible dependence of the maximum intensification rate on surface drag coefficient in reasonable range. However, a strong sensitivity of TC intensification to surface drag coefficient is found in the weak intensity stage, as also shown in previous full-physics model simulations (e.g., Kilroy et al. 2017; Peng et al. 2018; Li and Wang 2021a). This sensitivity can be explained by a tendency of the increasing degree of congruence between the moist entropy surface and the absolute angular momentum surface in the eyewall ascent as a result of the increasing boundary layer mass convergence with increasing surface drag coefficient and thus surface friction (Wang et al. 2021b) or a tendency of increasing inner-core inertial stability and the dynamical efficiency of eyewall heating (Wang et al. 2021a). Note that the refinements documented in this study mainly make the theory self-contained and feasible to examine the sensitivity of the theoretical TC potential intensification rate on various physical parameters/processes. Comparisons of the TC intensification rates and intensity evolutions estimated by the simple theory with those in the full-physics model simulations under different model parameters, including SST, the RMW of the initial TC vortex, drag coefficient, lateral and vertical mixing lengths, can be found in Wang et al. (2021a,b). Some comparisons of the theory with observations can be found in Xu and Wang (2022) and Wang et al. (2022).

In addition, to further demonstrate the validity of the constructed isothermal expansion effect in the simple theoretical framework, we compared two ensemble experiments using the full-physics, axisymmetric cloud model CM1 with the results shown in Fig. 15. One includes the time-dependent sea surface pressure in the calculation of sea surface saturation enthalpy and one with the constant unperturbed environmental sea surface pressure. The model settings are identical to the SST-dependent sounding experiments in Li et al. (2020) with an SST of 30ºC and atmospheric sounding sorted over the North Atlantic, but with the horizontal mixing length reduced from 700 m to 63 m to ensure the simulated TC strong enough so that the effect of isothermal expansion can be well observed. Dissipative heating is not included in the two ensemble experiments. We can see from Fig. 15 that without considering the pressure dependence (isothermal expansion effect) of sea surface saturation enthalpy results in a slightly smaller intensification rate and a 10% reduction in the maximum intensity of the simulated TC averaged during the quasi-steady state evolution. The difference between the two experiments is consistent with that predicted by the simple theoretical model as shown in Fig. 11. The time-dependent solutions of the TC intensity obtained by time integration of Eqs. (18)–(20) using the environmental parameters in the ensemble simulations are also shown in Fig. 15. We can see that the theoretical solutions well capture the TC intensity evolutions in the two ensemble experiments. The theoretical solutions are initialized when the TC intensity reached 17 m s^{-1} to reduce the effect of initial spinup of the numerical model (Li et al. 2020). In addition, the upper limit of the wind dependent C_D in CM1 is reduced from 2.4×10^{-3} to 2.0×10^{-3} in the theoretical solutions to capture the high steady-state intensity due to the use of a small horizontal mixing length in the numerical experiments. The results demonstrate that the theoretical model with the refinements in this study can capture the effect the pressure dependence of sea surface saturation enthalpy and reproduce the time evolution of the simulated TC intensity.

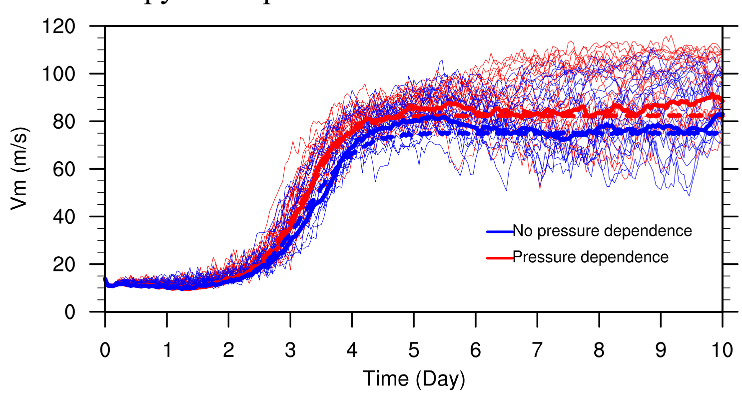

Fig. 15. The intensity evolutions in two ensemble experiments using the full-physics axisymmetric CM1, with results from the individual runs and ensemble mean shown in thin and thick curves (solid). The model settings are identical to those used in the SST-dependent sounding experiment in Li et al. (2020) with an SST of 30°C and atmospheric sounding sorted over the North Atlantic, but with the horizontal mixing length reduced from 700 m to 63 m. One experiment includes the pressure dependence of sea surface saturation enthalpy (red) and the other does not (blue). Dissipative heating is not included in the two experiments. The time-dependent solutions of TC intensity from Eqs. (18)–(20) using the environmental parameters in the ensemble simulation are shown in dashed thick curves.

Finally, we should point out that some issues need to be considered when the simple theory documented in this study is applied to real or numerically simulated TCs or when it is further developed in future studies. First, previous studies have shown the dependence of TC intensification rate on the structure of the initial TC vortex in both observations and full-physics model simulations (Xu and Wang 2015, 2018a,b; Li and Wang 2021b; Peng and Fang 2021; Li et al. 2022). As we mentioned in section 2b, no explicit structure parameter is included in the current version of the simple theoretical time-dependent equation of TC intensification. The parameters c in Eq. (14) and A in Eq. (19) can be modified to consider the possible dependence of TC intensification rate on TC structure. In that case, parameter c and the functional relationship between the parameters A and the TC relative intensity need to be recalibrated using both idealized full-physics model simulations and observations. The parameter c depends weakly on the inner-core dynamical structure of the TC. The form of A in the current theoretical framework does not strongly depend on the TC inner-core size (see Figs. 9c,d in Wang et al. 2021a). Second, the relationship between the outflow-layer air temperature and SST fitted in this study is based on the current climate, and it should be modified if the theory is applied to understand the impact of global warming on TC intensification and MPI, which is a topic under investigation. In addition, there is considerable variability in the outflow-layer air temperature relative to the fitted curve. Although part of the variability in the estimated outflow-layer temperature might be related to TC intensity, our preliminary analysis shows that the variability of the estimated outflow-layer air temperature is not related to TC intensity (not shown). It is likely related to the large-scale environmental flow patterns, which needs to be examined in a future study. In addition, the global reanalysis data could not capture the real TC intensity due to the relatively coarse resolution of the model used to produce the reanalysis data. We also noticed that in a recent theoretical study Rousseau-Rizzi and Emanuel (2021) assumed the weak temperature gradient (WTG) with the outflow layer temperature being independent of local SST. In that case, not only the possible dependence of the outflow-layer temperature on local SST but also the possible effect of the variability of the outflow temperature on TC MPI are ignored. Therefore, it is a good topic for a future study to evaluate the uncertainties related to the variability of the outflow-layer air temperature in estimating TC intensification rate and the steady-state intensity in the simple theoretical model. Our results also strongly suggest that the variability of air-sea temperature difference may be one of the major environmental factors that contribute to the observed variability of TC MPI and intensification rate even for a given SST (Xu et al. 2019a,b; Xu and Wang 2022).

Acknowledgments.

The authors are grateful to three anonymous reviewers for their constructive review comments, which helped improve the manuscript. This study was supported in part by National Natural Science Foundation of China under grant 41730960 and the National Key R&D Program of China under grant 2017YFC1501602 and in part by NSF grant AGS-1834300.

Data Availability Statement.

The EBT data were obtained from https://rammb2.cira.colostate.edu/research/tropical-cyclones/tc_extended_best_track_dataset/. The ERA-Interim data were obtained from https://apps.ecmwf.int/datasets/. The CM1 source code and model data used in this study are available at the website: https://box.nju.edu.cn/d/f0898f30cbee44c88adb/.

REFERENCES

Asselin, R., 1972: Frequency filter for time integrations. *Mon. Wea. Rev.*, **100**, 487-490, https://doi.org/10.1175/1520-0493(1972)100<0487:FFFTI>2.3.CO;2

Bister, M. and Emanuel, K.A., 2002. Low frequency variability of tropical cyclone potential intensity 1. Interannual to interdecadal variability. *J. Geophys. Res.*, *107*, 4801. https://doi:10.1029/2001JD000776.

Bryan, G. H., and J. M. Fritsch, 2002: A benchmark simulation for moist nonhydrostatic numerical model. *Mon. Wea. Rev.*, **130**, 2917–2928, https:/doi.org/10.1175/1520-0493(2002)130<2917:ABSFMN>2.0.CO;2.

Dee, D. P., and Coauthors, 2011: The ERA-Interim reanalysis: Configuration and performance of the data assimilation system. *Quart. J. Roy. Meteor. Soc.*, **137**, 553–597, https://doi.org/10.1002/qj.828.

Demuth, J. L., M. DeMaria, J. A. Knaff, and T. H. Vonder Haar, 2004: Evaluation of advanced microwave sounding unit tropical-cyclone intensity and size estimation algorithms. *J. Appl. Meteor. Climatol.*, **43**, 282–296, https://doi.org/10.1175/1520-0450(2004)043%3C0282:EOAMSU%3E2.0.CO;2.

Edwards, J. M. 2019: Sensible heat fluxes in the nearly neutral boundary layer: The impact of frictional heating within the surface layer. *J. Atmos. Sci.*, **76**, 1039-1053. https://doi.org/10.1175/JAS-D-18-0158.1.

Emanuel, K. A., 1986: An air-sea interaction theory for tropical cyclones. Part I: Steady-state maintenance. *J. Atmos. Sci.,* **43**, 585–605, https:/doi.org/10.1175/1520-0469(1986)043<0585:AASITF>2.0.CO;2.

Emanuel, K. A., 1988: The maximum intensity of hurricanes. *J. Atmos. Sic*., **45**, 1143–1155, https://doi.org/10.1175/1520-0469(1988)045<1143:TMIOH>2.0.CO;2.

Emanuel, K. A., 1995: Sensitivity of tropical cyclones to surface exchange coefficients and a revised steady-state model incorporating eye dynamics. *J. Atmos. Sci*., **52**, 3969-3976, https://doi.org/10.1175/1520-0469(1995)052<3969:SOTCTS>2.0.CO;2.

Emanuel, K. A., 2012: Self-stratification of tropical cyclone outflow: Part II: Implications to storm intensification. *J. Atmos. Sci*., **69**, 988–996, https://doi.org/10.1175/JAS-D-11-0177.1.

Emanuel, K., 2017: A fast intensity simulator for tropical cyclone risk analysis. *Nat. Hazards*, **88**, 779–796, https://doi.org/10.1007/s11069-017-2890-7.

Kieu, C. 2015: Revisiting dissipative heating in tropical cyclone maximum potential intensity. *Quart. J. Roy. Meteor. Soc*., **141**, 2497–2504, https://doi.org/10.1002/qj.2534.

Kilroy, G., M. T. Montgomery, and R. K. Smith, 2017: The role of boundary-layer friction on tropical cyclogenesis and subsequent intensification. *Quart. J. Roy. Meteor. Soc.*, **143**, 2524–2536. https://doi.org/10.1002/qj.3187.

Landsea, C. W., and J. L. Franklin, 2013: Atlantic hurricane database uncertainty and presentation of a new database format. *Mon. Wea. Rev.*, **141**, 3576–3592, https://doi.org/10.1175/MWR-D-12-00254.1.

Li, T.-H., and Y. Wang, 2021a: The role of boundary layer dynamics in tropical cyclone intensification. Part I: Sensitivity to surface drag coefficient. *J. Meteor. Soc. Japan*, **99**, 537–554, https://doi.org/10.2151/jmsj.2021-027.

Li, T.-H., and Y. Wang, 2021b: The role of boundary layer dynamics in tropical cyclone intensification. Part II: Sensitivity to initial vortex structure. *J. Meteor. Soc. Japan*, **99**, 555–573, https://doi.org/10.2151/jmsj.2021-028.

Li, Y., Y. Wang, Y. Lin, and R. Fei, 2020: Dependence of superintensity of tropical cyclones on SST in axisymmetric numerical simulations. *Mon. Wea. Rev*., **148**, 4767–4781, https://doi.org/10.1175/MWR-D-20-0141.1.

Li, Y., Y. Wang, and Z.-M. Tan, 2022: Why does the initial wind profile inside the radius of maximum wind matter to tropical cyclone development? *J. Geophys. Res.–Atmos.*, **127**, e2022JD037039, https:/doi.org/10.1029/2022JD037039.

Ozawa, H., and S. Shimokawa, 2015: Thermodynamics of a tropical cyclone: generation and dissipation of mechanical energy in a self-driven convection system. *Tellus A*, **67**, 24216, https://doi.org/10.3402/tellusa.v67.24216.

Peng, K., R. Rotunno, and G. H. Bryan, 2018: Evaluation of a time-dependent model for the intensification of tropical cyclones. *J. Atmos. Sci.*, **75**, 2125–2138, https://doi.org/10.1175/JAS-D-17-0382.1.

Peng, K., and J. Fang, 2021: Effect of the initial vortex vertical structure on early development of an axisymmetric tropical cyclone. *J. Geophys. Res.–Atmos.,* **126**, e2020JD033697, doi:10.1029/2020JD033697.

Rotunno, R., and K. A. Emanuel, 1987: An air-sea interaction theory for tropical cyclones. Part II. *J Atmos Sci*, **44**, 542–561, https://doi.org/10.1175/1520-0469(1987)044<0542:AAITFT>2.0.CO;2.

Rousseau-Rizzi, R. and Emanuel, K., 2021. A weak temperature gradient framework to quantify the causes of potential intensity variability in the tropics. *J. Climate*, **34**, 8669–8682, https://doi.org/10.1175/JCLI-D-21-0139.1.

Wang, Y., and J. Xu, 2010: Energy production, frictional dissipation, and maximum intensity of a numerically simulated tropical cyclone. *J. Atmos. Sci.*, **67**, 97–116, doi:10.1175/2009JAS3143.1.

Wang, Y., Y.-L. Li, J. Xu, Z.-M. Tan, and Y.-L. Lin, 2021a: The intensity-dependence of tropical cyclone intensification rate in a simplified energetically based dynamical system model. *J. Atmos. Sci.*, **78**, 2033–2045, https://doi.org/10.1175/JAS-D-20-0393.1.

Wang, Y., Y. Li, and J. Xu, 2021b: A new time-dependent theory of tropical cyclone intensification. *J. Atmos. Sci*., **78**, 3855–3865, https://doi.org/10.1075/JAS-D-21-0169.1.

Wang, Y., J. Xu, and Z.-M. Tan, 2022: Contribution of dissipative heating to the intensity-dependence of tropical cyclone intensification. *J. Atmos. Sci.*, **79**, 2169–2180, https://doi.org/10.1175/JAS-D-22-0012.1.

Xu, J., and Y. Wang, 2015: A statistical analysis on the dependence of tropical cyclone intensification rate on the storm intensity and size in the North Atlantic. *Wea. Forecasting*, **30**, 692–701, https://doi.org/10.1175/WAF-D-14-00141.1.

Xu, J., Y. Wang, and Z.-M. Tan, 2016: The relationship between sea surface temperature and maximum potential intensification rate of tropical cyclones over the North Atlantic. *J. Atmos. Sci.*, **73**, 4979–4988, https://doi.org/10.1175/JAS-D-16-0164.1.

Xu, J., and Y. Wang, 2018: Dependence of tropical cyclone intensification rate on sea surface temperature, storm intensity, and size in the western North Pacific. *Wea. Forecasting*, **33**, 523–537, https://doi.org/10.1175/WAF-D-17-0095.1.

Xu, J., Y. Wang, and C. Yang, 2019a: Factors affecting the variability of maximum potential intensity (MPI) of tropical cyclones over the North Atlantic. *J. Geophys. Res.: Atmos.,* **124**, 6654–6668. https://doi.org/10.1029/2019JD030283.

Xu, J., Y. Wang, and C. Yang, 2019b: Interbasin differences in the median and variability of tropical cyclone MPI in the northern hemisphere. *J. Geophys. Res.: Atmos.*, **124**, 13,714–13,730, https://doi.org/10.1029/2019JD031588.

Zeng, Z., L.-S. Chen, and Y. Wang, 2008: An observational study of environmental dynamical control of tropical cyclone intensity in the North Atlantic. *Mon. Wea. Rev.*, **136**, 3307–3322, https://doi.org/10.1175/2008MWR2388.1